Electronic Supplementary Material (ESI) for Journal of Materials Chemistry B.

Supporting Information

Conductive Polyacrylamide Hydrogel Enabled by Dispersion-Enhanced MXene@Chitosan Assembly for Highly Stretchable and Sensitive Wearable Skin

Yaqing Liu[a], Daren Xu[b], Yi Ding[a], Xiaoxiao Lv[a], Tingting Huang[a], Bolei Yuan[a], Lin Jiang[a], Xueying Sun[a], Yuanqing Yao[a] and Jun Tang[a]*

[a]Department of Polymer Science, College of Chemistry, Jilin University, Changchun 130012, China

[b]State Key Laboratory of Supramolecular Structure and Materials, Jilin University, Qianjin Avenue 2699, Changchun 130012, P. R. China

*Address correspondence to: chemjtang@jlu.edu.cn (J. Tang)

Zeta potential (mV) Viscosity / Concentration	5-20 mpa•s	50-100 mpa•s	100-200 mpa•s	200-400 mpa•s
0	-32.25			
1.125	44.6	41.6	41.6	36
1.875	53.8	52.4	50.2	43.7
2.625	59.9	59.2	54.2	43.9

Table S1 Zeta potential of MXene solution doped with chitosan of different concentrations and viscosities (the concentration of MXene is 1.2 mg/mL).

Conductivity Viscosity (x10^{-4} S/cm) / Concentration	5-20 mpa•s	50-100 mpa•s	100-200 mpa•s	200-400 mpa•s
0				
1.125	28.8			
1.875	32.8	19.4		
2.625	15.8	33.1	24.9	

Table S2 Conductivity of DEMH doped with chitosan of different concentrations and viscosities (the concentration of MXene is 2.8 mg/mL).

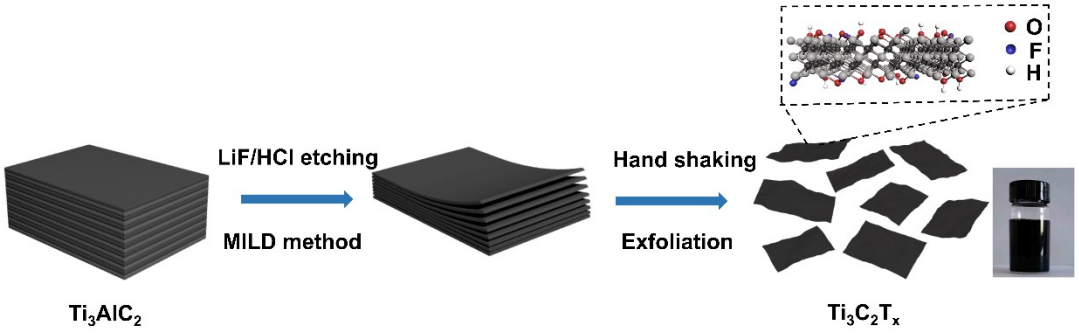

Fig. S1 Schematic for the synthesis of the MXene nanosheets.

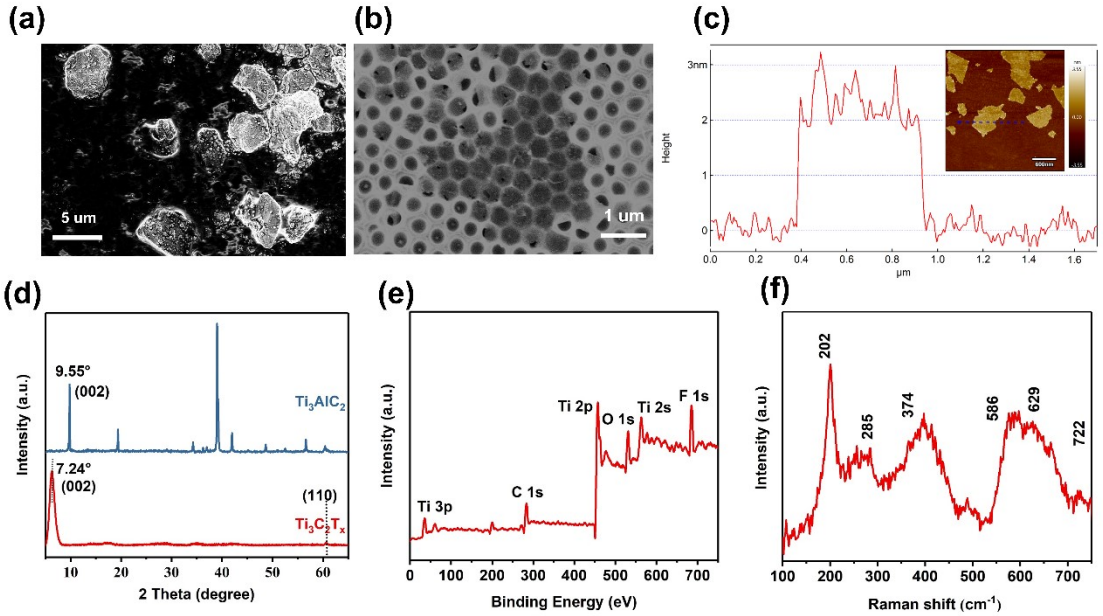

Fig. S2 (a) SEM image of Ti_3AlC_2. (b) TEM image of MXene nanosheet in porous alumina substrate. (c) AFM image of the conductive MXene nanosheet. (d) XRD patterns of Ti_3AlC_2 and $Ti_3C_2T_x$. (e) XPS spectrum of $Ti_3C_2T_x$. (f) Raman spectrum of $Ti_3C_2T_x$.

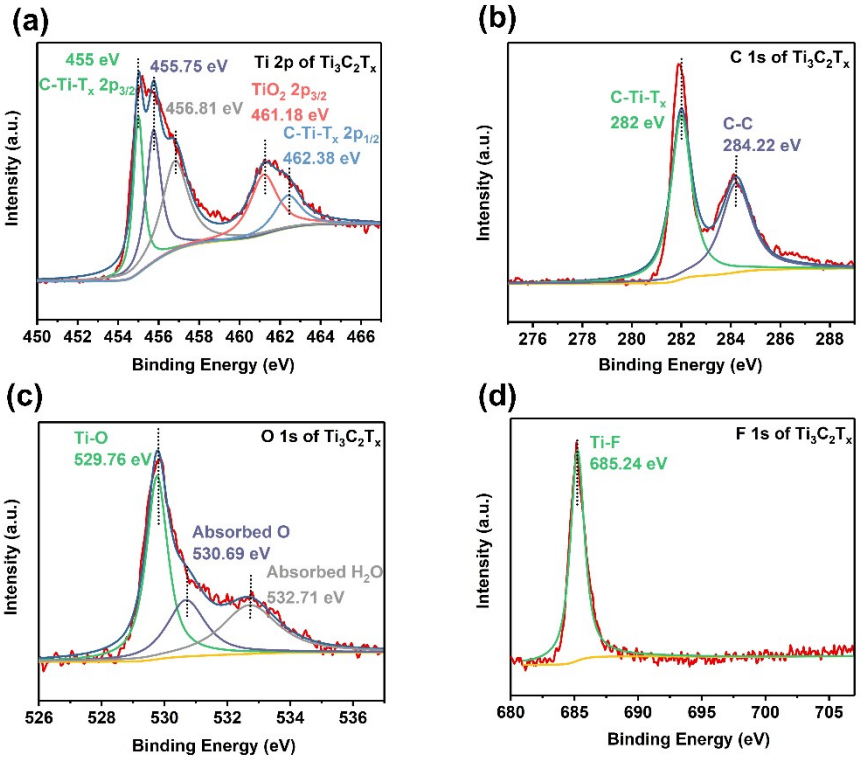

Fig. S3 (a) XPS spectrum of the $Ti_3C_2T_x$ in Ti 2p region. (b) XPS spectrum of $Ti_3C_2T_x$ in C 1s region. (c) XPS spectrum of $Ti_3C_2T_x$ in O 1s region. (d) XPS spectrum of $Ti_3C_2T_x$ in F 1s region.

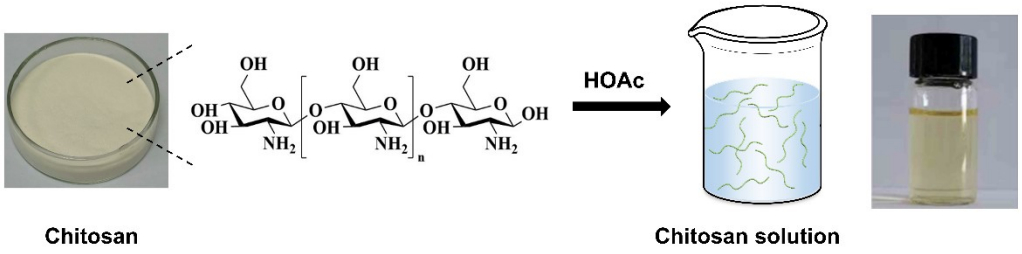

Fig. S4 Schematic for the synthesis of chitosan liquid.

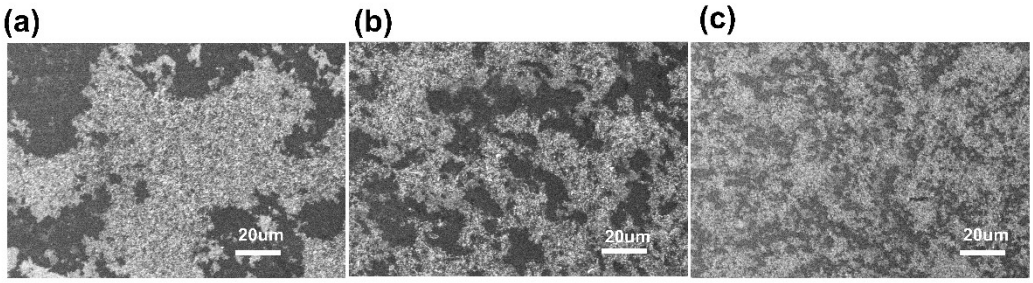

Fig. S5 (a) SEM image of $Ti_3C_2T_x$. (b) SEM image of MXene@125Chitosan. (c) SEM image of MXene@250Chitosan.

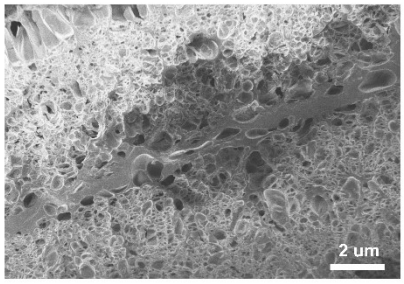

Fig. S6 SEM image of self-healing DEMH1.2.

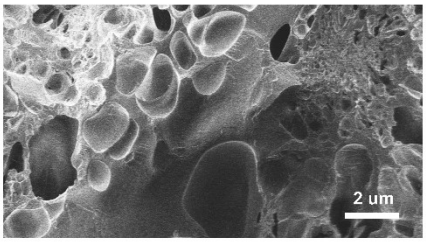

Fig. S7 SEM image of MPAM.

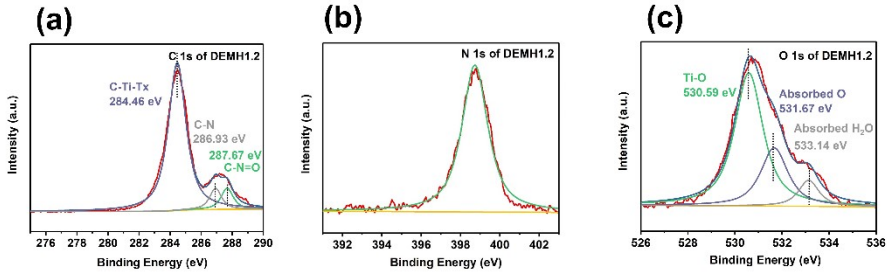

Fig. S8 (a) XPS spectrum of DEMH1.2 in C 1s region. (b) XPS spectrum of DEMH1.2 in N 1s region. (c) XPS spectrum of DEMH1.2 in O 1s region.

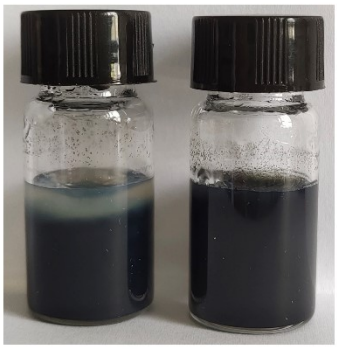

Fig. S9 The digital photos of MPAM and DEMH1.2**.**

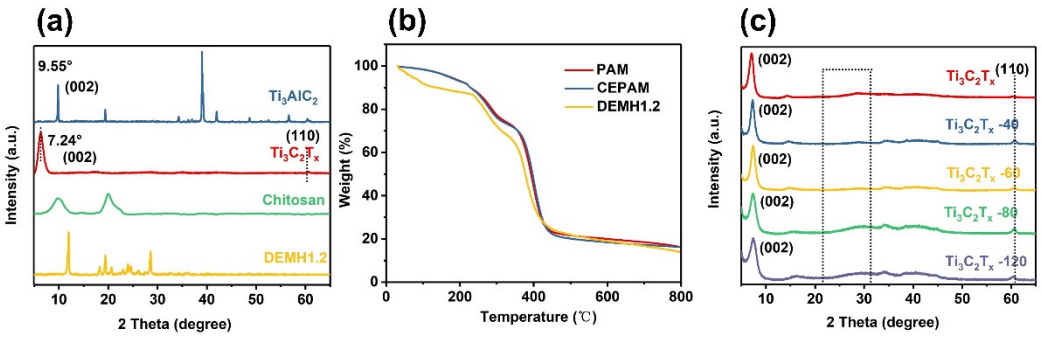

Fig. S10 (a) XRD patterns of Ti_3AlC_2, $Ti_3C_2T_x$, chitosan and DEMH1.2. (b) TGA curves of PAM, CEPAM and DEMH1.2. (c) XRD patterns of $Ti_3C_2T_x$, $Ti_3C_2T_x$ -40, $Ti_3C_2T_x$ -60, $Ti_3C_2T_x$ -80, $Ti_3C_2T_x$ -120.

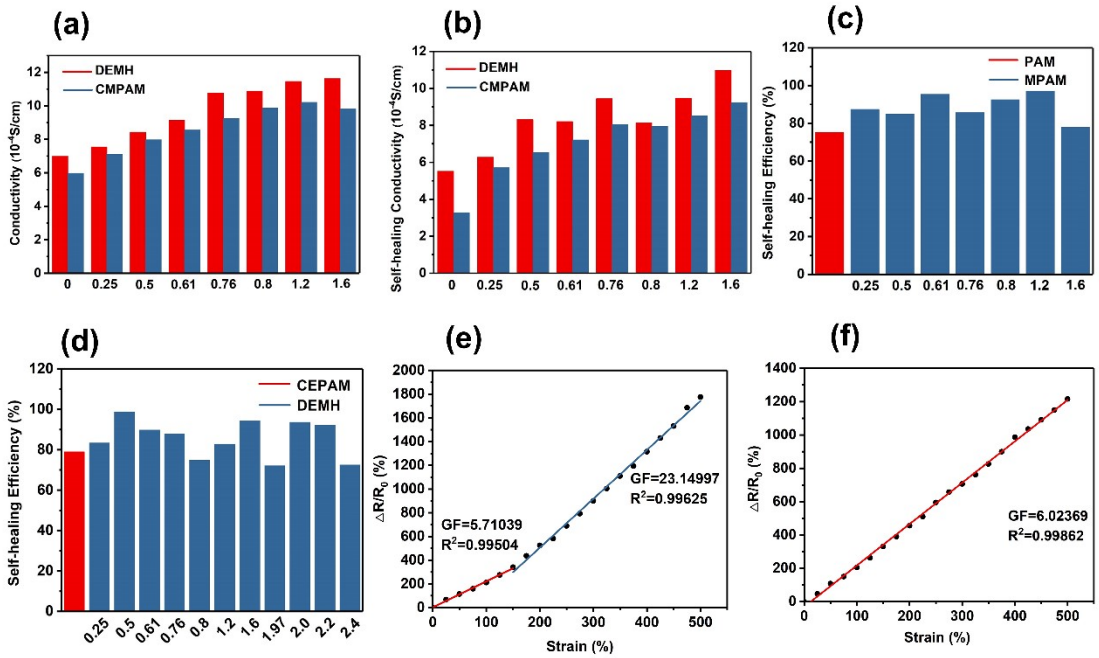

Fig. S11 (a) Conductivity of CMPAM and DEMH in different mass ratio of MXene. (b) Self-healing conductivity of CMPAM and DEMH in different mass ratio of MXene. (c) Self-healing efficiency of MPAM in different mass ratio of MXene. (d) Self-healing efficiency of DEMH in different mass ratio of MXene. (e) Gauge factor of MPAM. (f) Gauge factor of DEMH1.2.

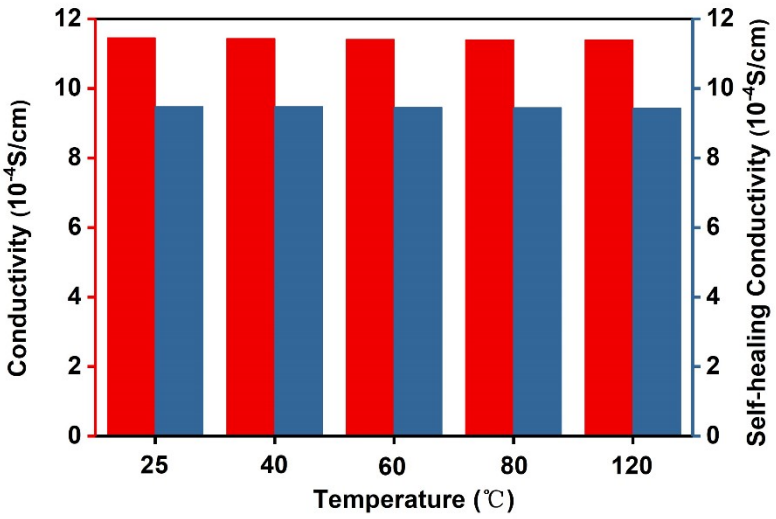

Fig. S12 Conductivity and Self-healing conductivity of DEMH1.2 in different temperatures for 24 h.

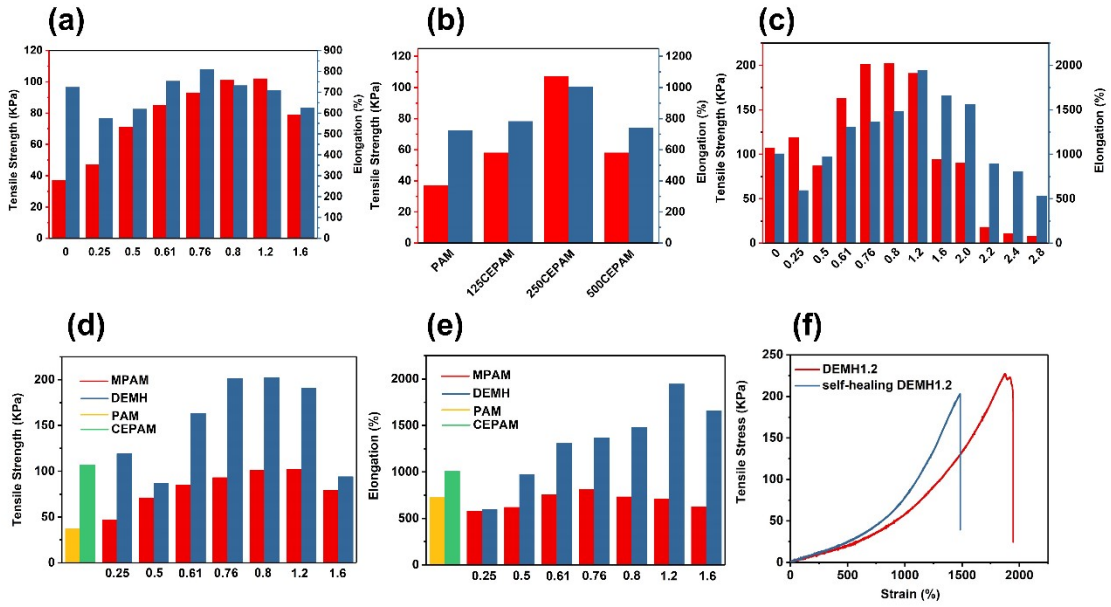

Fig. S13 (a) Tensile stress-strain curves of MPAM in different mass ratio of MXene. (b) Tensile stress-strain curves of CEPAM in different mass ratio of chitosan. (c) Tensile stress-strain curves of DEMH in different mass ratio of MXene with the same ratio of chitosan. (d-e) Tensile stress-strain curves and elongation of DEMH and MPAM in different mass ratio of MXene and chitosan. (f) Tensile stress-strain curves of DEMH1.2 and self-healing DEMH1.2.

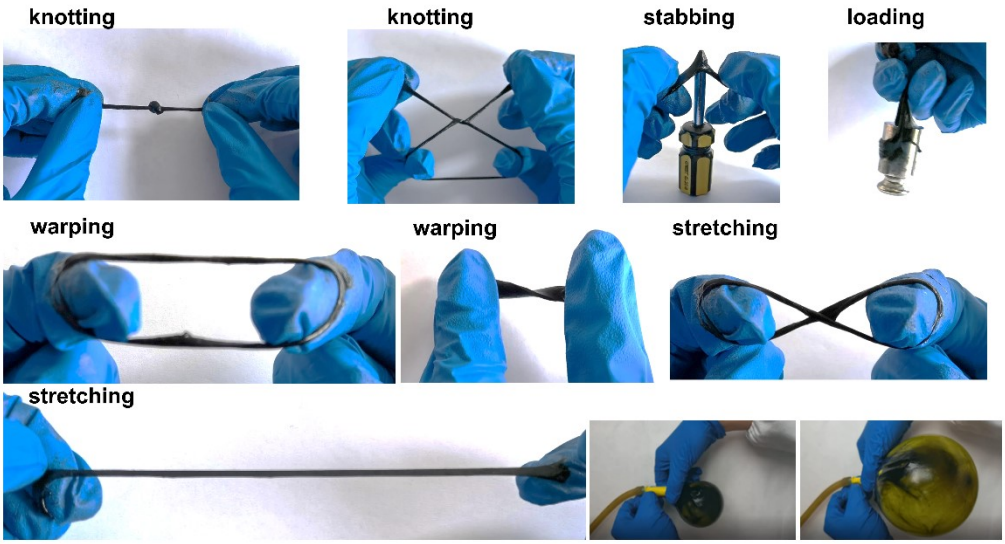

Fig. S14 Exhibition of superior mechanical properties for DEMH, including knotting, stabbing, loading, warping and stretching.

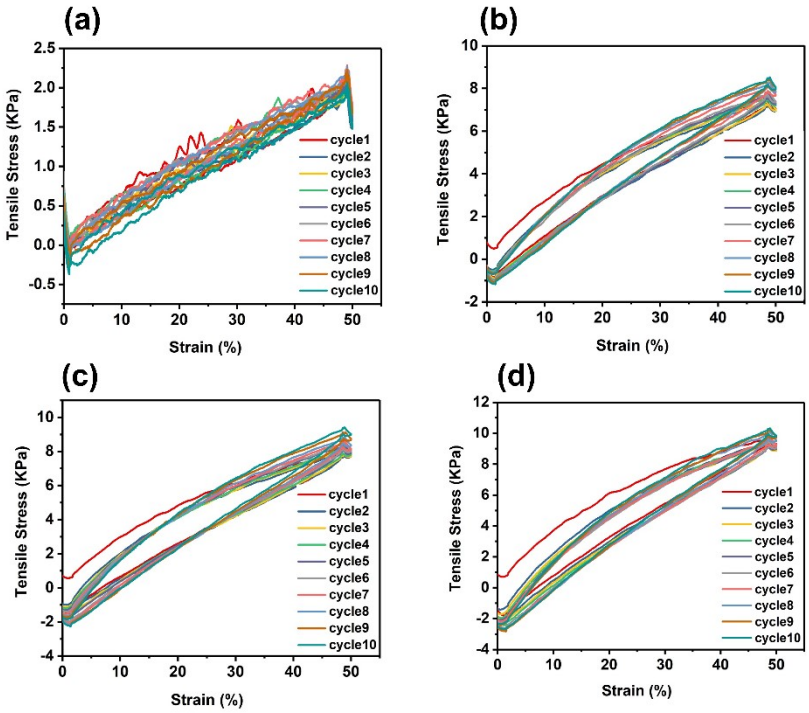

Fig. S15 (a) Tensile loading-unloading tests of PAM at different setting strains 50%. (b) Tensile loading-unloading tests of CEPAM at different setting strains 50%. (c) Tensile loading-unloading tests of MPAM at different setting strains 50%. (d) Tensile loading-unloading tests of DEMH at different setting strains 50%.

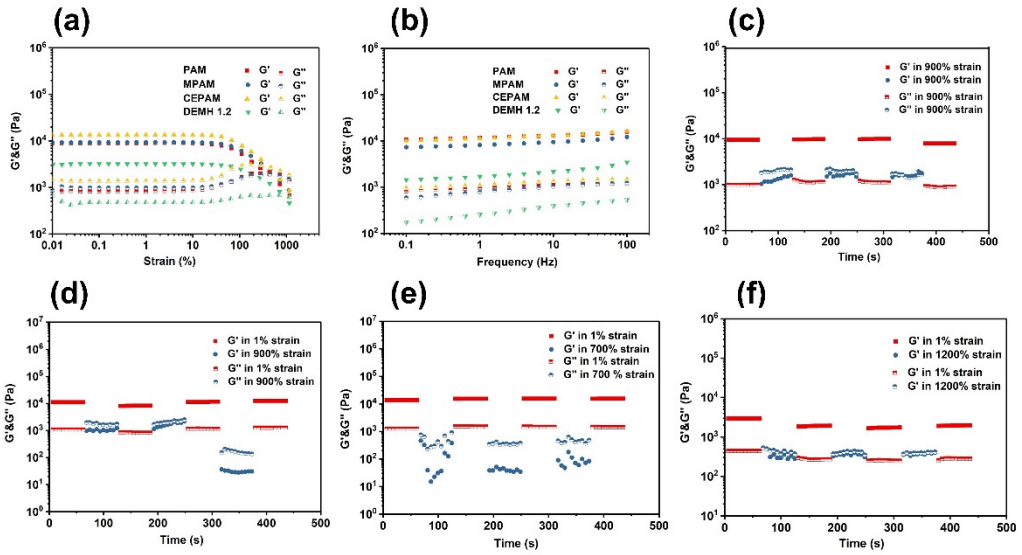

Fig. S16 (a) The G’ and G’’ of the hydrogel from strain amplitude sweep (γ = 0.01%–1000%) at a fixed angular frequency (10 rad•s $^{-1}$). (b) G’ and G” of the hydrogel in the oscillatory frequency sweep test. (c) The G’ and G’’ of the PAM when alternate step strain switched from small strain (γ = 1.0%) to large strain (γ = 900%) at a fixed angular frequency (10 rad•s $^{-1}$), each strain interval was kept as 60 s. (d) The G’ and G’’ of the CEPAM when alternate step strain switched from small strain (γ = 1.0%) to large strain (γ = 900%) at a fixed angular frequency (10 rad•s $^{-1}$), each strain interval was kept as 60 s. (e) The G’ and G’’ of the MPAM when alternate step strain switched from small strain (γ = 1.0%) to large strain (γ = 700%) at a fixed angular frequency (10 rad•s $^{-1}$), each strain interval was kept as 60 s. (f) The G’ and G’’ of the DEMH when alternate step strain switched from small strain (γ = 1.0%) to large strain (γ = 1200%) at a fixed angular frequency (10 rad•s $^{-1}$), each strain interval was kept as 60 s.

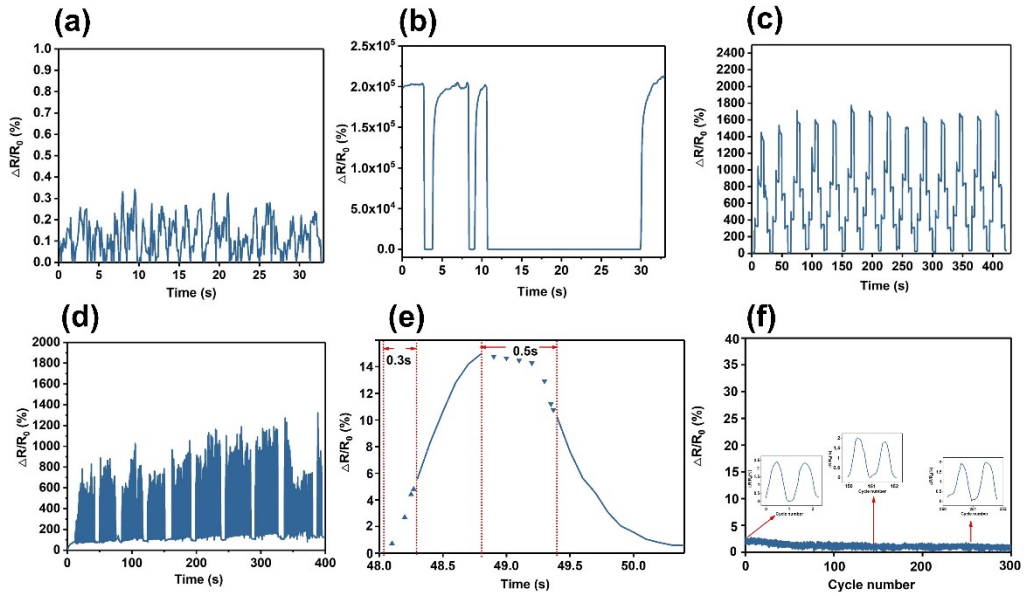

Fig. S17 (a) Speak 'Hello' repeatedly. (b) Dissection and self-healing. (c) Stretch different proportions. (d) Stretch repeatedly. (e) Response and relaxation time of DEMH1.2. (f) Response of DEMH1.2 to repeated loading and unloading 300 cycles, showing the good stability of this strain sensor.